The submitted manuscript has been created by the University of Chicago as Operator of Argonne National Laboratory ("Argonne") under Contract No. W-31-109-ENG-38 with the U.S. Department of Energy. The U.S. Government retains for itself, and others acting on its behalf, a paid-up, nonexclusive, irrevocable worldwide license in said article to reproduce, prepare derivative works, distribute copies to the public, and perform publicly and display publicly, by or on behalf of the Government.

Proceedings of
ASME Turbo Expo 2002
June 3-6, 2002, Amsterdam, The Netherlands

GT-2002-30645

NONDESTRUCTIVE CHARACTERIZATION OF ENVIRONMENTAL BARRIER COATINGS APPLIED TO MONOLITHIC CERAMICS

W. A. Ellingson, C. Deemer, S. Erdman and A. Parikh
Energy Technology Division
Argonne National Laboratory
Argonne, Il 60439

ABSTRACT

Full-size silicon nitride gas-turbine vanes coated with an environmental barrier coating (EBC) were evaluated in an exploratory way by two nondestructive methods: polarized elastic optical scattering and infrared thermal imaging. Initial test results indicate that the laser scatter data correlate with EBC thickness. A description of the methods and results of recent tests are presented.

INTRODUCTION

Environmental barrier coatings (EBCs) are under development to reduce oxidation damage to monolithic ceramic components that are used in the high-temperature operating environments of gas-fired turbine engines. Nondestructive evaluation (NDE) methods are under development to assess the condition of EBCs before their insertion into an engine, as well as to assess damage accumulated during service. Noncontact, polarized, back-scattered laser light and one-sided infrared imaging NDE methods which previously were shown to be effective on EBCs on composites have been tested on a proprietary-composition EBC on AS800 Si_3N_4. The AS800 vanes were developed for service in a natural-gas-fired turbine engine.

EBC-COATED VANES

The EBC ceramic vanes, see Fig. 1, were about 3 cm high with an aerodynamic chord of about 27 mm. The proprietary EBC was applied using a plasma spray method, and the thickness of the EBC, estimated from destructive cross-sections were estimated to be about 50-70 µm. Two vanes examined by NDE methods were in the as-received condition, and the other vanes were examined after having been run in the Rolls-Royce/Allison 501-KB 4MWe field engine in Mobile, AL, for up to 1621 hours (Ref. 2). The vanes were installed as first-stage vanes where operating temperatures of about 1182ºC were expected.

The surface finish of the as-received vanes were not smooth and had several surface features that were apparent by visual inspection. Prior work (Ref. 3) has demonstrated that surface finish effects on thermal barrier coatings (TBCs) will impact substrate material temperatures as well as rates of erosive wear. The EBC vanes that had been in-service in the Rolls-Royce/Allison engine had regions where visual inspection indicated the EBC had eroded away as can be seen in Fig. 1.

(a) (c)

(b) (d)

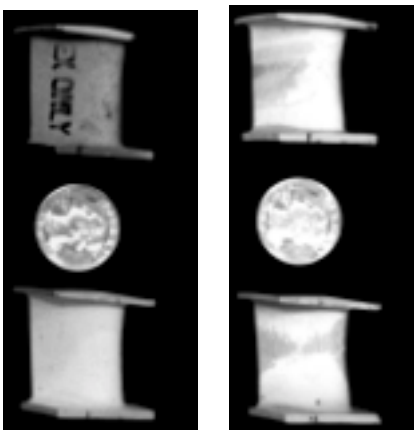

Figure 1. Photographs of four monolithic ceramic vanes with an EBC: (a) as-received vane, (b) after 542 h, and (c, d) after 1621 h (note the erosive wear regions).

EXPERIMENTAL METHODS

Two NDE methods were used to provide exploratory examination of the EBC monolithic vanes: a polarized elastic optical scattering based on reflectometry (Refs. 4, 5, 6) and one-sided infrared thermal imaging (Refs. 7, 8). The polarized optical method, described fully elsewhere (Ref. 5), relies on several characteristics related to the materials to be studied. One characteristic is that the material to be studied must be optically

 Copyright © #### by ASME

translucent at the wavelength or wave-lengths of interest. We have conducted a through-transmission optical characterization of the as-deposited EBC, as well as materials similar to that deposited on the AS800 monolithic material. Figure 2 shows the optical transmission characteristics of material closely related to the EBC applied. Note that there is a small optical transmission at 0.633 µm, which is the wavelength of the helium-neon laser we use. However, higher transmission can be achieved by use of longer wavelengths, such as our Ti: sapphire solid-state laser that provides up to 0.92 µm. These were not scanned at 0.92 µm because of experimental issues. These are now resolved. Another characteristic of optical scattering is that changes in the polarization angle of scattered light allow study of different scattering mechanisms (Refs. 9, 10), as is the case in a layered structure typical of a monolithic ceramic with an EBC. Figure 3 shows a diagram of such a layered structure with a defect within the EBC. In the figure, arrows show the angle of incidence of the probing laser light as well as angle of scatter.

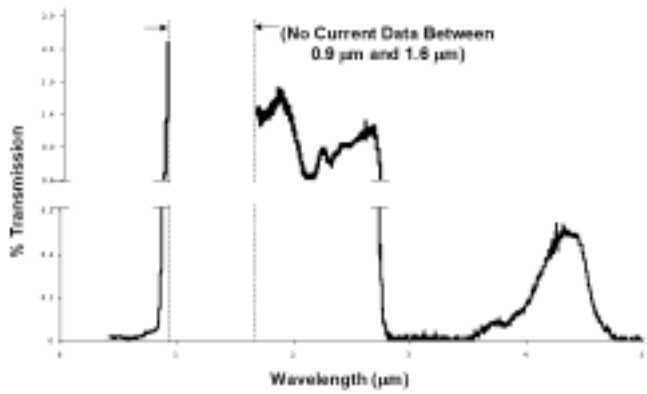

Figure 2. Normalized optical transmission characteristics of EBC similar to that deposited on monolithic Si_3N_4.

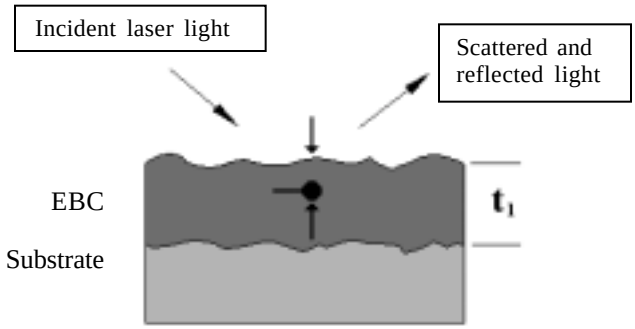

Figure 3. Schematic of a layered structure similar to a monolithic ceramic with an EBC of thickness, t_i.

Most work to date reported in the literature has used angle-of-incidence scattering, as shown in Fig. 4a. In our work, we do not use an angle of incidence, rather we use a normal incidence similar to conventional reflectometry as shown in Figure 4b. Our experience with thermal barrier coatings (TBCs) of yttria-stabilized zirconia (Ref. 1) has demonstrated that normal incidence works very well for detection of delaminations (Ref. 7). An example of debond detection of an electron-beam physical vapor deposited (EB-PVD) TBC, is shown in Figs. 5 and 6. Figure 5 is a schematic diagram of a 25 mm diameter specimen, a diagram showing the laser impulse method used to generate delams at the TBC/substrate (Ref. 10), and a steady-state thermal image showing locations of delams. Figure 6a shows resulting back-scatter laser test results showing delam detection at the several spots where the pulsed laser induced delams. Figure 6b is the result of one-sided flash thermal imaging on the same specimen. Note that the 75 mj pulse seeen on the laser back-scatter is not clearly detected by the one-sided thermal flash. These results suggested that similar approaches might succeed on EBCs, if optical properties would be appropriate.

The second NDE method, one-sided thermal imaging, is shown in Fig. 7. In this method, the thermal flash unit and the infrared camera are both placed on the same side of the specimen. Time-sequential surface temperature maps are obtained over a pre-set field of view. For the EBC-coated vanes, the field of view used was the entire vane, about 27 mm by 30 mm.

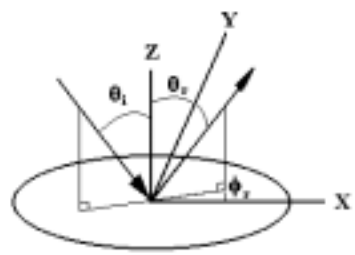

(a)

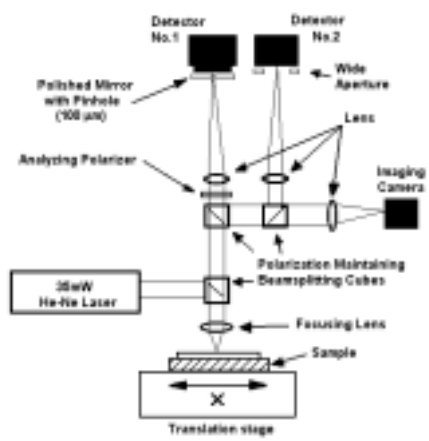

(b)

Figure 4. Schematics of two polarized elastic optical scatter setups: (a) angle-of-incidence scattering, (b) normal incidence scattering.

Copyright © #### by ASME

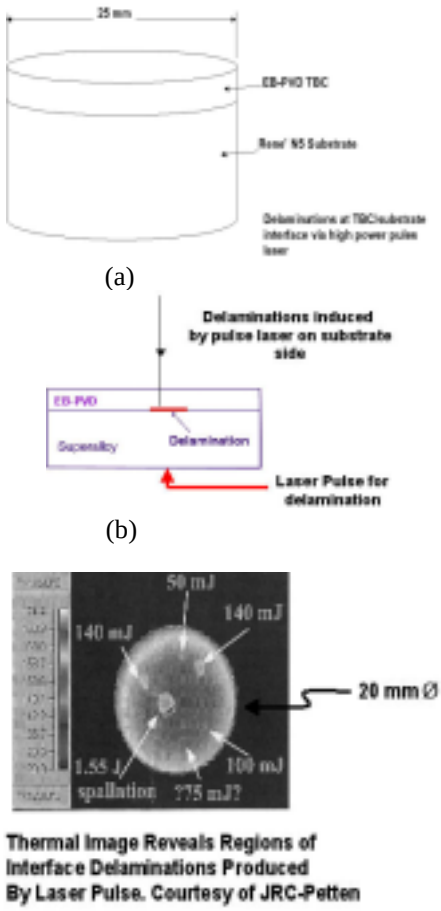

Figure 5. EB-PVD test sample used for initial NDE studies: (a) schematic diagram of sample, (b) schematic diagram showing test setup for generation of debonds, and (c) steady-state thermal image showing locations of debonds.

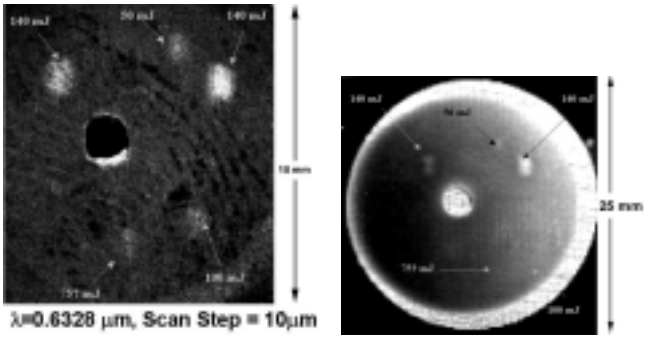

(a) (b)

Figure 6. NDE test results from TBC specimen of Fig. 5. (a) laser backs scatter, (b) one-sided IR.

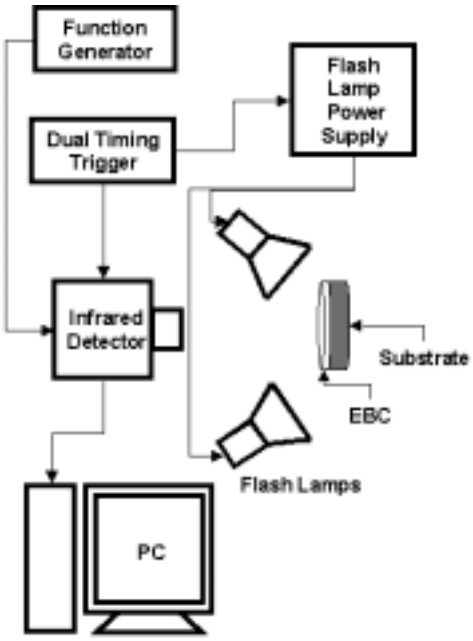

Figure 7. Schematic diagram showing one-sided thermal imaging experimental set up.

RESULTS

One of the as-received vanes had a small, < 1mm, spalled region, as shown in Fig. 8. What was unknown was if a larger region existed around the spall where a future spall could be expected. By raster scanning the laser over the region of the spall, back-scatter data suggested the region that might be expected to spall. The resulting scatter "image" data are shown in Fig. 9a.

Figure 8. Photograph showing location on vane where the visible spall had occurred.

Copyright © #### by ASME

(a)

(b)

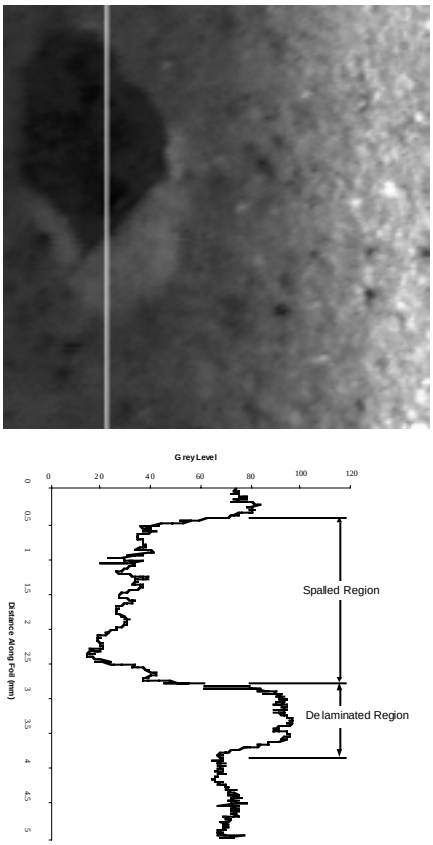

Figure 9. Laser scatter image data showing extent of suspected delaminated region: (a) laser scatter data image with white line showing where line profile obtained, (b) line plot across laser scatter image as noted showing suspected delaminated region.

The same test sample was examined by one-sided thermal imaging. Figure 10 shows time-sequential thermal images of the region near the visible spall. Surface temperature data were obtained with a high-frame-rate infrared camera. In these tests, we used a focal-plane array camera which had image rates up to 2000 frames per second. Tests conducted on these samples used 500 frames per second. The first few milliseconds of image data are saturated so typically image data are displayed after the feature can be defined.

Surface temperature as a function of time after flash across a particular region of interest is shown in Fig. 11. Delaminated areas would have a much lower rate of thermal decay than the surrounding area. Vanes and other complex shapes, however, must be treated carefully because of directional effects.

To verify if any disbonding had occurred near the suspect delamination region, the vane was sectioned and optical photomicrographs obtained. Figure 12 shows that the region around the visible spall was not delaminated but rather the thickness of the EBC changed, and thus, the NDE data suggest a thickness change, not delamination.

(a) (b) (c) (d)

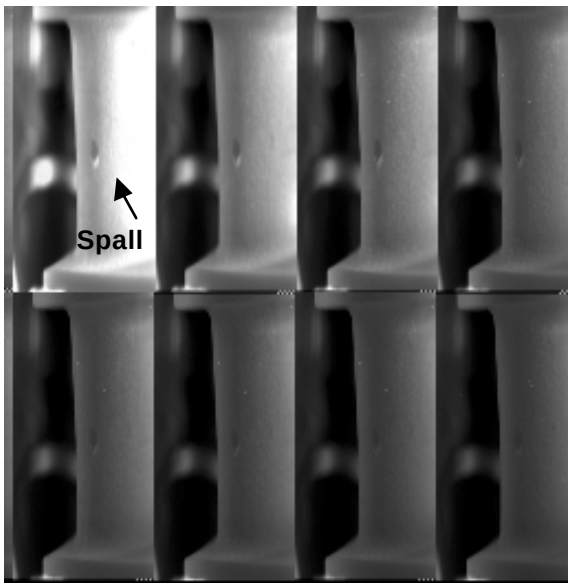

(e) (f) (g) (h)

Figure 10. Time-dependent surface temperature images showing the region near the spall where suspected delamination might be present. Time after flash: a) 0.04 s, b) 0.05 s, c) 0.06 ss, d) 0.08 s, e) 0.10 s, f) 0.12 s, g) 0.14, h) 0.16 s.

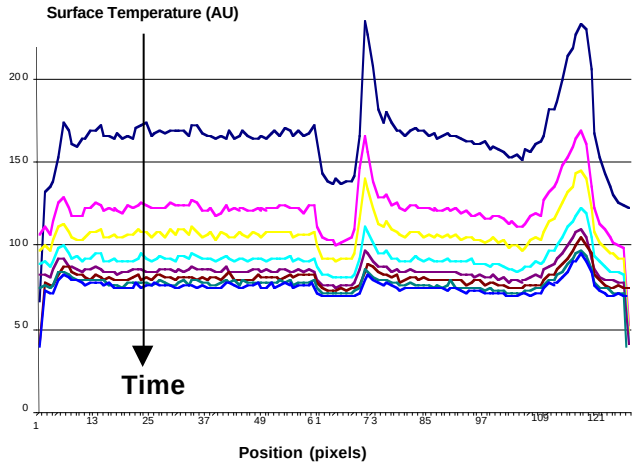

Figure 11. Surface-temperature time plots near the spalled region.

Copyright © #### by ASME

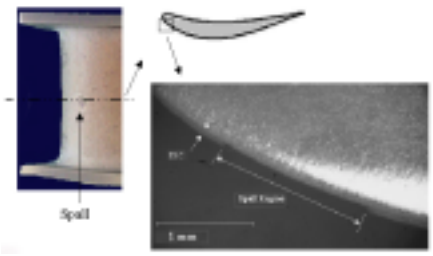

(a)

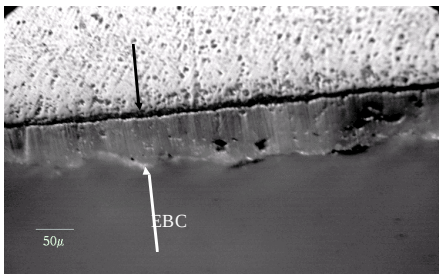

(b)

Figure 12. Destructive analysis near the spalled region: (a) photograph of vane showing spalled region, and (b) optical photomicrograph of region noted in “a”.

Three other vanes with an EBC were examined as a function of engine run times. Three vanes were examined with the laser scatter, one after 542 hours and two after 1621 hours. Figure 13a shows the 20 by 22-mm region on the vanes that were scanned with the laser. Figures 13b-13d are the resulting gray-scale image data typical of what results from the laser scans with 13b being the data from the as-received vane, 13c are the data from the 542 hour vane and 13d are the data from the 1621 hour vane. To be noted in Fig. 13b is that the as-received vane had been stamped with an ink marker. The laser scatter data are sensitive to such surface characteristics and this or similar markings cause 'noise' in the resulting data. Figure 14 shows a series of plots of the image gray scale data from Fig.13. Each plot represents the gray scale value as a function of distance from the top platform. Note that the laser data were not obtained for the entire distance between platforms. Three positions were selected on each gray scale image as a function of the distance from the leading edge. These were 5 mm, 15 mm and 22 mm. Three positions were selected because it seemed clear that there was a difference in the coating condition as the distance from the leading edge increased. Fig. 14a are the data for the vane in the as-received condition, 14b are for the vane after exposure for 542 hours and 14c are the data for one of the 1621 hour vanes. Unfortunately, none of the vanes that were run in the engine had a before-exposure reference data set.

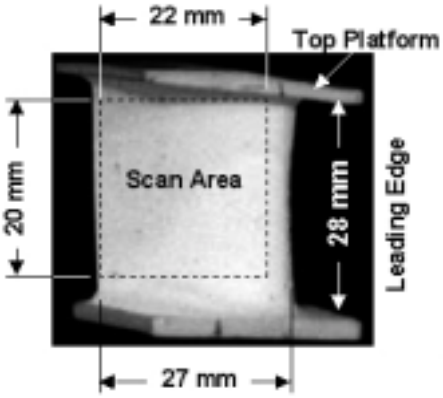

(a)

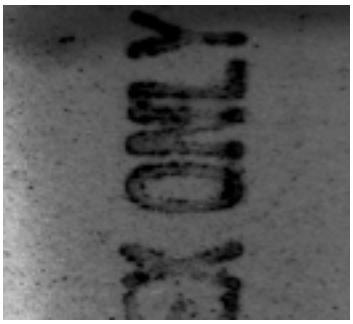

(b)

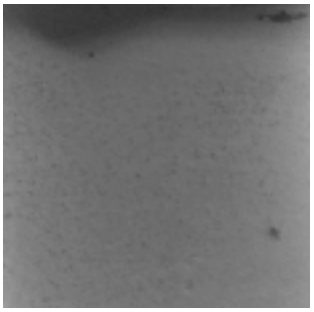

(c)

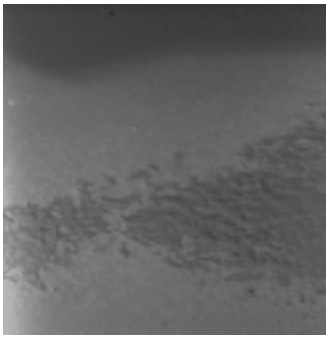

(d)

Figure 13. Laser scatter data. (a) Diagram showing region over which laser scatter gray-scale data were obtained, (b) laser scatter data for as-received vane with markings, (c) laser scatter gray-scale data for 542 hr vane, and (d) laser scatter gray-scale data for one 1621 hr vane.

Copyright © #### by ASME

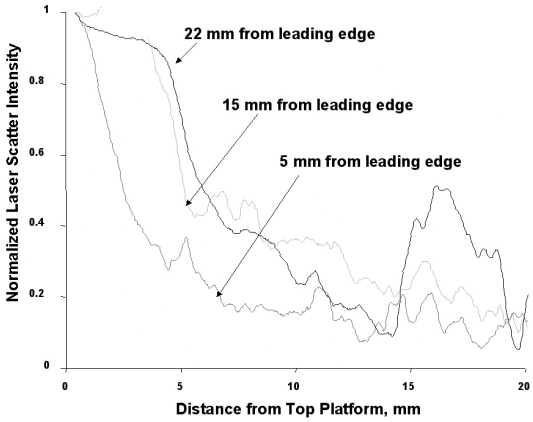

(a)

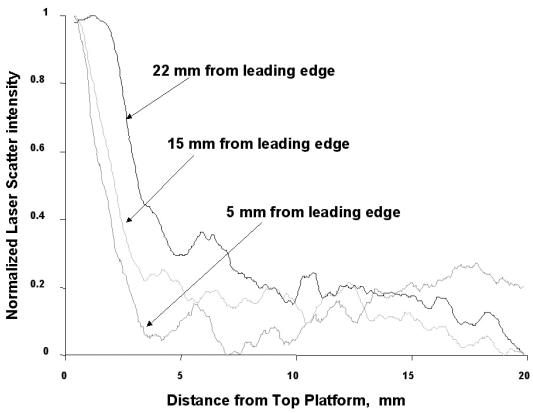

(b)

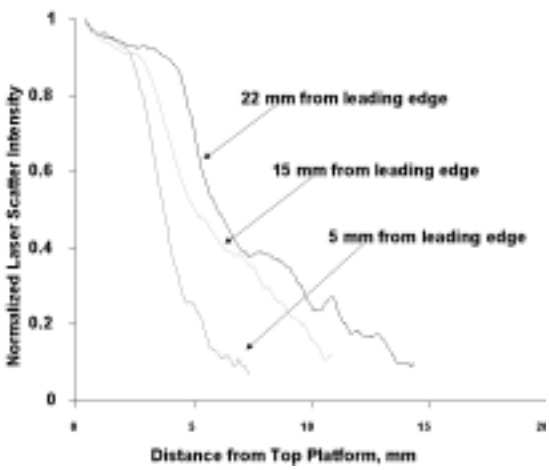

(c)

Figure 14. Resulting gray-scale line plots from laser scatter data. (a) Three positions on as-received vane, (b) three positions on 524 hr vane, and (c) three positions on 1621 hr vane.

However, several features can be observed from these data sets. First is that there is an apparent non-uniformity to the as-produced coating thickness between platforms with the coating getting thicker near the platforms. Second, after 542 hours, the coating thickness variations change with the coating getting more uniform probably reflecting the velocity profile across the vane. Third, while difficult to quantify, the laser data has less noise at 1621 hours which correlates with visible observations that the surface finish is much smoother in the coating regions that remained in tact.

On the basis of the scatter intensity data as a function of position between the platforms, the laser scattered light intensity seems to be related to the local thickness of the EBC. Thus, if a baseline data set were obtained with a calibration of scatter intensity as a function of thickness, it might be possible to map the changes in thickness of the EBC. This thickness map could be useful as information on which to base re-use/replace or strip and re-coat decisions.

CONCLUSIONS

Five monolithic Si_3N_4 ceramic vanes with a proprietary EBC were examined in an exploratory way by NDE. The NDE methods used had been shown previously to detect delaminations and pre-spall conditions for thermal barrier coatings and EBCs on ceramic composites. The vanes examined included two which were in the as-received condition and three which had been run in a natural-gas-fired turbine. Two NDE methods were used: one based on laser scattering using a modified reflectometer setup and one based on time-dependent infrared thermal imaging using a one-sided setup. The preliminary results suggest that the polarized back-scatter method has sensitivity to changes in EBC thickness that might be caused by erosive wear. This observation is based on results of erosive-wear patterns of EBCs from test engines. The preliminary results also suggest that the NDE results need to be carefully examined because similar results might be obtained between a delaminated specimen and a specimen that has an EBC thickness change. This will need to be studied more carefully in order to establish which of these coating characteristics is the controlling parameter.

REFERENCES

1 Ellingson, W. A., Deemer, C., Parikh, A., and Erdman, S., "Development of Nondestructive Evaluation Technology for High-Temperature Coatings," proc. of 15th Annual Conference on Fossil Energy Materials, Knoxville, TN, April 30-May 2, 2001.

2 Wenglarz, R. A., " Rolls-Royce Allison Ceramic Vane Project," Proc. of the 1998 Advanced Turbine Systems Annual Program Review Meeting, US Department of Energy, November 2-4, 1998.

3 Soechting, F. O., "A Design Perspective on Thermal Barrier Coatings," NASA Conf. pub. 3312, pp. 1-15, 1995.

4 Ellingson, W. A., Todd, J. A., and Sun, J. G., "Optical Method and Apparatus for Detection of Defects and Microstructural Changes in Ceramics and Ceramic Coatings," US patent number 6,285,449, issued September 4, 2001.

5 Ellingson, W. A., and Sun, J. G., " Automated Real-Time Detection of Defects during Machining of

Copyright © #### by ASME

Ceramics," US patent number 5,689,332, issued November 18, 1997.

6 Tompkins, H. G., and McGahan, W. A., "Spectroscopic Ellipsometry and Reflectometry," John Wiley and Sons, Inc., New York, 1999.

7 Deemer, C., Sun, J. G., Ellingson, W. A., and Short, S., "Front-Flash Thermal Imaging Characterization of Continuous Fiber Ceramic Composites," Cer. Eng. Sci., Vol. 20, No. 3, pp. 317-324, 1999.

8 Ellingson, W. A., Sun, J. G., More, K. L., and Hines, R., "Characterization of Melt Infiltrated SiC/SiC Composite Combustor Liners using Meso and Micro NDE Techniques," ASME paper GT-2000-0067, International Gas Turb. Conf., Munich, Germany, May, 2000.

9 Germer, T. A., "Polarized Light Scattering by Microroughness and Small Defects in Dielectric Layers," J. Op. Soc. Am., Vol. 18, No. 6, pp. 1279-1288, 2001.

10 Arias-Gonzales, J. R., Nieto-Vesperinas, M., and Madrazo, A., "Morphology-Dependent Resonances in the Scattering of Electromagnetic Waves from an Object Buried Beneath a Plane or a Random Rough Surface," J. Op. Soc. Am., Vol. 16, No. 12, pp 2928-2934, 1999.

11 Karlsson, A. M., Levi, C. G., and Evans, A. G., "A Model Study of Displacement Instabilities During Cycle Oxidation," ACTA MAT (in press).

Copyright © #### by ASME